Expanded View Figures

Figure EV1. Annotated sequence alignment for coronavirus PLpro.

Sequence alignment generated with T-coffee/ESPRIPT (Gouet *et al*, 2003; Magis *et al*, 2014) aligning PLpro sequences from SARS2, SARS and MERS. Sequence numbering and secondary structure elements are shown according to the high-resolution apo structure of SARS-CoV-2 PLpro (pdb 6wrh, unpublished). T, turn. Domains and subdomains are boxed in different colours, and catalytic triad, as well as residues mutated in this study, is indicated.

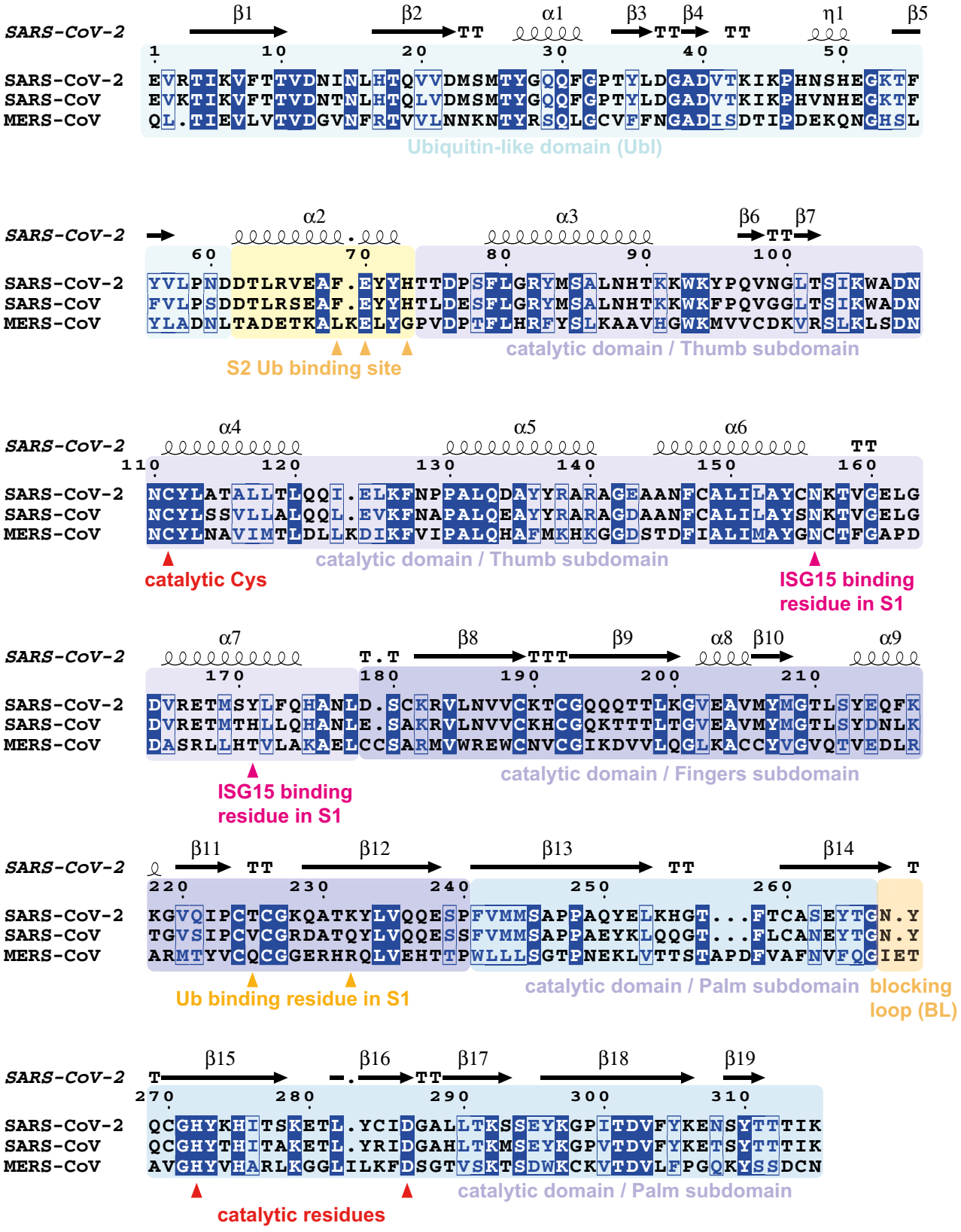
SARS-CoV-2
SARS-CoV-2
SARS-CoV
MERS-CoV
Ubiquitin-like domain (Ubl)
S2 Ub binding site
catalytic domain / Thumb subdomain
catalytic Cys
ISG15 binding residue in S1
catalytic domain / Fingers subdomain
Ub binding residue in S1
catalytic domain / Palm subdomain
blocking loop (BL)
catalytic residues

Figure EV1.

Figure EV2. Selection of available structures of coronavirus PLpro.

A large body of work on SARS and MERS PLpro has led to determination of multiple structures of PLpro apo and PLpro bound to ubiquitin and ISG15. When multiple structures were available, the highest resolution structure was used.

A *left*, the unpublished structure of apo SARS2 PLpro (pdb 6wrh, 1.6 Å, determined by the Centre for Structural Genomics of Infectious Disease (CSGID)) is coloured in analogy with Figs 1E and EV1, indicating Thumb, Fingers and Palm subdomain. The PLpro fold forms an open right hand that holds the ubiquitin fold, guiding its C-terminus into the active site. PLpro contains an N-terminal Ubl domain of unknown function, and this domain can vary in orientation. The high-resolution structure was generated with a catalytic Cys to Ser mutation; a more common catalytic Cys to Ala mutant destabilises PLpro (Fig EV3D). *Middle*, structure of SARS2 PLpro bound to ubiquitin (orange, covered by a semi-transparent surface). *Right*, structure of SARS2 PLpro bound to the C-terminal domain of ISG15 ($ISG15^{CTD}$, salmon, under a semi-transparent surface). Also see Fig 1. In ubiquitin and $ISG15^{CTD}$ complexes, propargylamide-based suicide probes (Ekkebus *et al*, 2013) covalently modify catalytic Cys111.

B *left*, SARS PLpro apo (1.85 Å, pdb 2fe8 (Ratia *et al*, 2006)), *middle*, SARS PLpro bound to ubiquitin (1.4 Å, pdb 4m0w (Chou *et al*, 2014)), *right*, SARS PLpro bound to the C-terminal domain of ISG15 (2.4 Å, pdb 5tl7 (Daczkowski *et al*, 2017a)).

C *left*, MERS PLpro apo (1.84 Å, pdb 4rna (Lee *et al*, 2015)), *middle*, MERS PLpro bound to ubiquitin (2.15 Å, pdb 4rf1 (Bailey-Elkin *et al*, 2014)), *right*, MERS PLpro bound to the C-terminal domain of ISG15 (2.4 Å, pdb 5w8u (Daczkowski *et al*, 2017b)).

D Superpositions of PLpro structures with S1 site occupied by different modifiers. Overall, PLpro shows high similarity, extending to the position and orientation of the N-terminal Ubl domain, with the notable exception of a distinct position of the Ubl in the SARS complex with $ISG15^{CTD}$ (pdb 5tl7 (Daczkowski *et al*, 2017a)). The second most variable region concerns the Fingers subdomain, which shows varying degrees of "openness." Superposition shows that the structures of SARS and SARS2 bound to individual modifiers are highly similar, and the modifiers adapt identical orientations and engage in similar interactions with PLpro. MERS PLpro seems to vary on the theme of ubiquitin versus ISG15 recognition, by binding both modifiers similarly. In the MERS ubiquitin complex, the Fingers are more closed, and the ubiquitin is pushed towards the Thumb domain, to adopt a similar orientation and interaction as seen for ISG15 bound to MERS. MERS PLpro ubiquitin complexes have been determined with "open" and more "closed" Fingers (Bailey-Elkin *et al*, 2014).

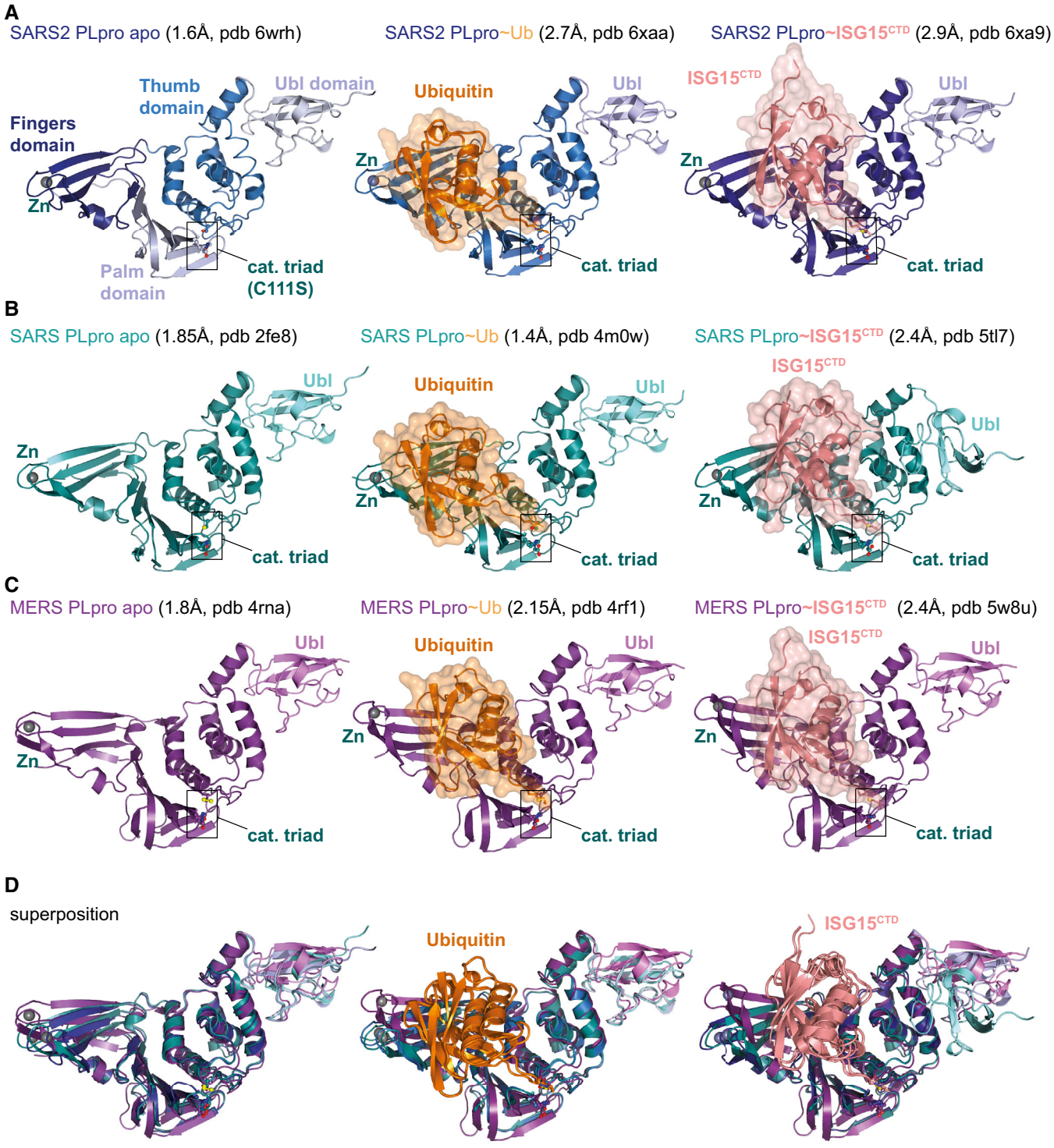
A
SARS2 PLpro apo (1.6Å, pdb 6wrh)
SARS2 PLpro~Ub (2.7Å, pdb 6xaa)
SARS2 PLpro~ISG15CTD (2.9Å, pdb 6xa9)
Thumb domain
Ubl domain
Fingers domain
Zn
Palm domain
cat. triad (C111S)
Ubiquitin
Ubl
cat. triad
ISG15CTD
B
SARS PLpro apo (1.85Å, pdb 2fe8)
SARS PLpro~Ub (1.4Å, pdb 4m0w)
SARS PLpro~ISG15CTD (2.4Å, pdb 5tl7)
C
MERS PLpro apo (1.8Å, pdb 4rna)
MERS PLpro~Ub (2.15Å, pdb 4rf1)
MERS PLpro~ISG15CTD (2.4Å, pdb 5w8u)
D
superposition

Figure EV2.

Figure EV3. Separation-of-function mutations in SARS2 PLpro.

A Ubiquitin and ISG15 binding site analysis based on PISA analysis, indicating interface residues on SARS2 PLpro.

B Superposition of Ub-PA (orange) and $ISG15^{CTD}$-PA (salmon) as bound to SARS2 PLpro highlights the different binding modes with a ~ 40° rotation between the two proteins.

C Details of the binding of $ISG15^{CTD}$ and the Thumb domain of SARS2 PLpro. Interacting residues shown as sticks.

D Mutations in S1 and S2 sites were introduced in PLpro, and the enzyme variants were expressed in bacteria, purified and tested for integrity by assessing the inflection temperature, indicating the transition of folded to unfolded protein. With exception of mutating the catalytic Cys to Ala, which was severely destabilised and precipitated during purification, all other mutants showed similar stability to wild-type PLpro. Inflection temperature values were determined in technical duplicate from experiments performed twice.

E, F Triubiquitin cleavage to mono- and diubiquitin (*left*) and proISG15 cleavage to mature ISG15 (*right*) were compared side-by-side over a time course, resolved on SDS–PAGE gels, and visualised by Coomassie staining. Experiments were performed in duplicate with 250 nM enzyme and 2 μM substrate; all gels are shown in Source Data. (E), Activity of wild-type PLpro, reproduced from Appendix Fig S1B and C, for comparison. (F), S1 site mutants as indicated. See Fig 2.

Source data are available online for this figure.

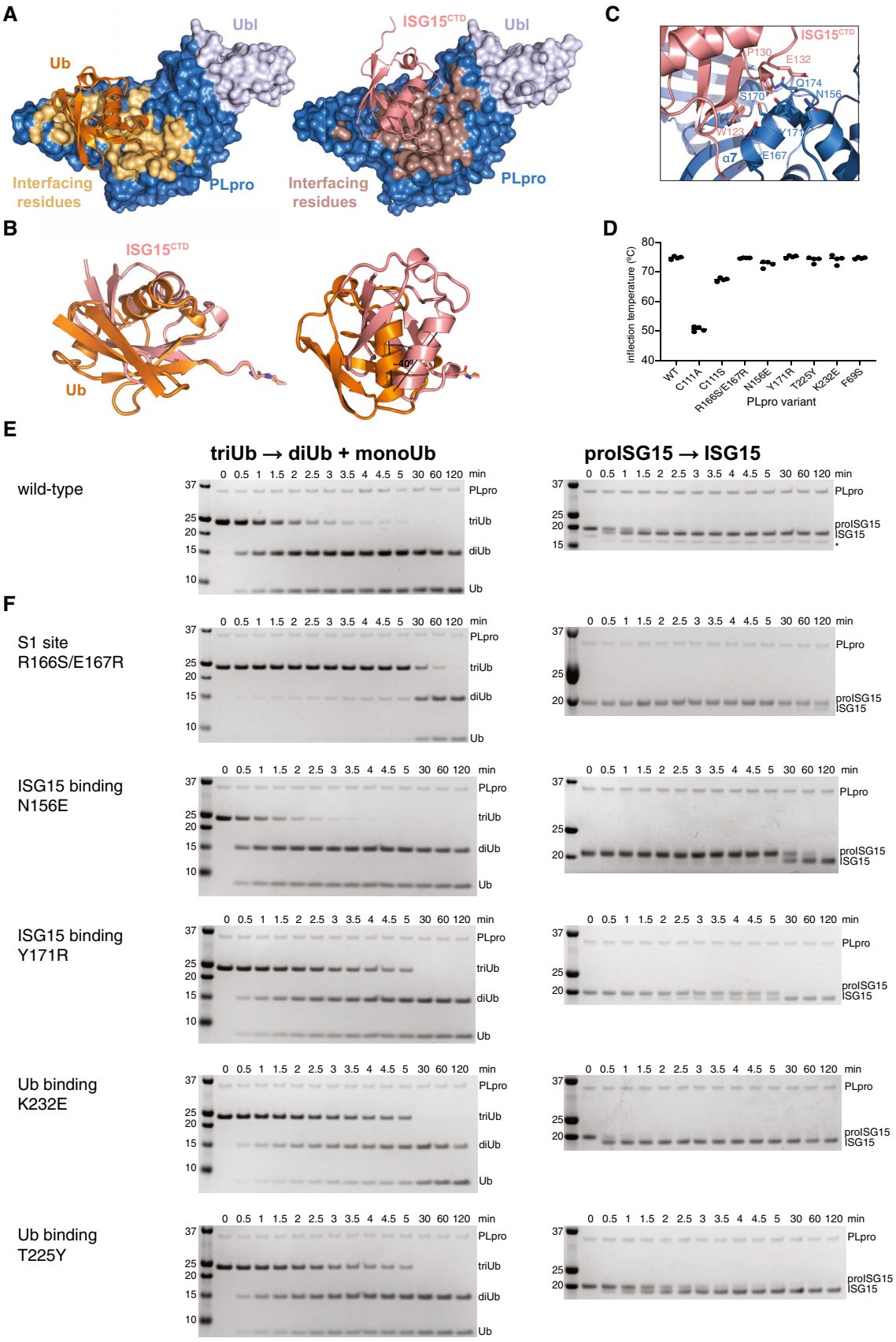
A
Ub
Ubl
Interfacing residues
PLpro
ISG15CTD
Ubl
Interfacing residues
PLpro
B
ISG15CTD
Ub
~40°
C
ISG15CTD
P130
E132
Q174
S170
N156
W123
Y171
α7
E167
D
inflection temperature (°C)
80
70
60
50
40
WT
C111A
C111S
R166S/E167R
N156E
Y171R
T225Y
K232E
F69S
PLpro variant
E
triUb → diUb + monoUb
proISG15 → ISG15
wild-type
0 0.5 1 1.5 2 2.5 3 3.5 4 4.5 5 30 60 120 min
37
25
20
15
10
PLpro
triUb
diUb
Ub
proISG15
ISG15
*
F
S1 site R166S/E167R
ISG15 binding N156E
ISG15 binding Y171R
Ub binding K232E
Ub binding T225Y

Figure EV3.

Figure EV4. Developing a high-throughput screen to identify SARS2 PLpro inhibitors.

A Suitable SARS2 PLpro concentrations were determined by kinetic analysis of increasing Ub-Rhodamine fluorescence over 1 h (3,600 s). Concentrations ranged from 10 to 5,000 nM with sufficient signal obtained with 50 nM SARS2 PLpro at a constant concentration of 100 nM Ub-Rhodamine. Maximal signal (Max) indicates pre-incubated Ub-Rhodamine with 25 nM PLpro for 1 h, to achieve complete cleavage of Ub-Rhodamine, before measurement.

B To determine the optimal substrate concentration, 50 nM SARS2 PLpro was incubated with 25–250 nM Ub-Rhodamine for 30 min (1,800 s). A final concentration of 100 nM Ub-Rhodamine was selected, which was well below K_M for SARS2 PLpro, in the linear range of the reaction, with a signal to background (S:B) above 3 at 12 min (720 s). 12 min was the timepoint selected for end-point assays.

C Enzymatic reactions were stopped with addition of citric acid at a final concentration of 10 mM at indicated timepoints. The assay was benchmarked against compound rac5c (see below, Figs 5 and EV5). Rac5c inhibited SARS2 PLpro activity with an IC_{50} of 0.81 μM (Fig 5C, see Materials and Methods, Appendix Table S1).

D Results from the complete screen, by plate number (also see Dataset EV1).

E Signal:background analysis from the whole screen by plate number. 17 out of 18 plates met the quality control criteria (S:B > 2).

F Robust Z′ analysis of the whole screen by plate number. Plate 6a, which did not meet quality criteria in S:B and robust Z′ analysis, was excluded from analysis.

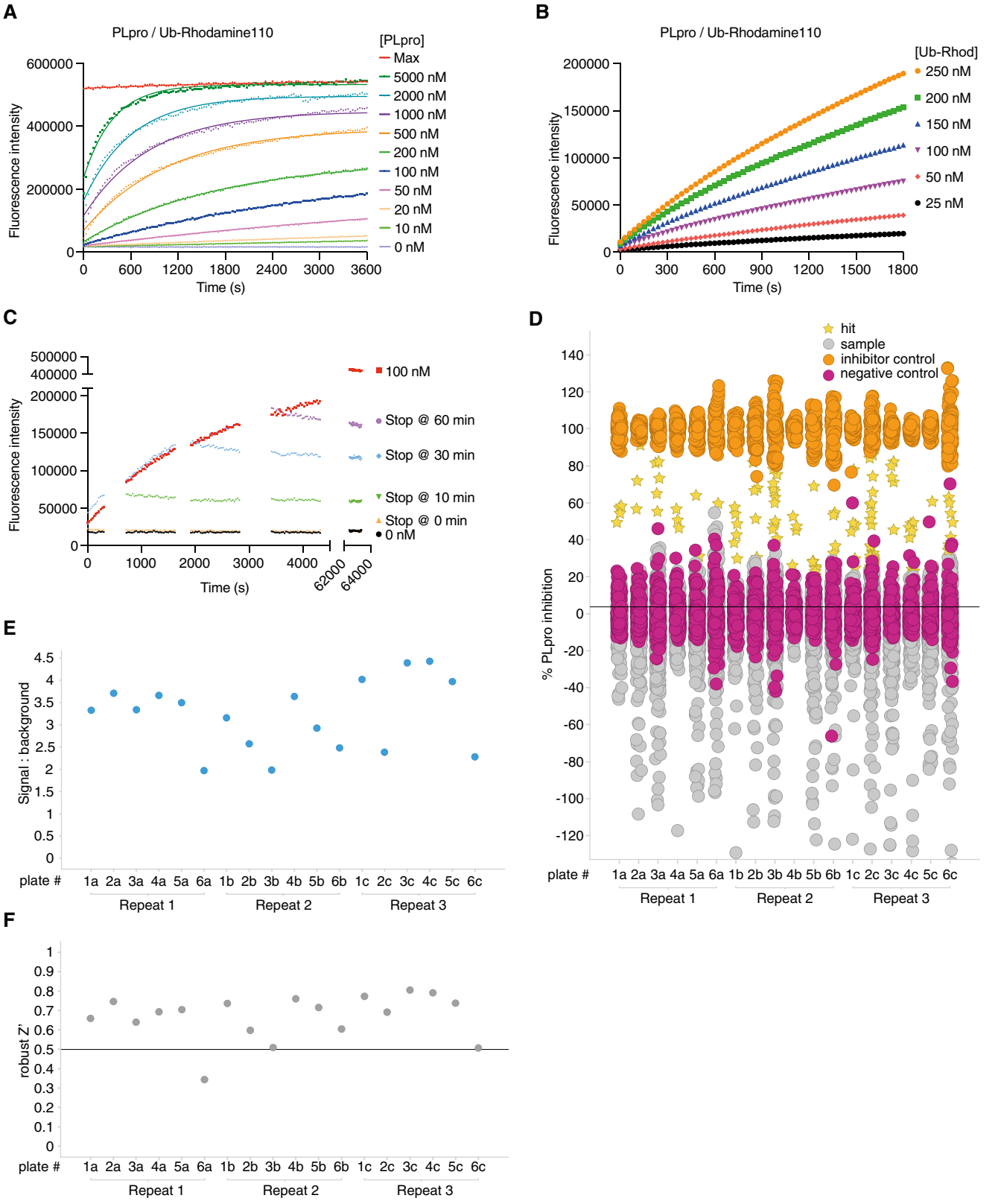
A
PLpro / Ub-Rhodamine110
[PLpro]
Max
5000 nM
2000 nM
1000 nM
500 nM
200 nM
100 nM
50 nM
20 nM
10 nM
0 nM
Fluorescence intensity
Time (s)
B
PLpro / Ub-Rhodamine110
[Ub-Rhod]
250 nM
200 nM
150 nM
100 nM
50 nM
25 nM
Fluorescence intensity
Time (s)
C
100 nM
Stop @ 60 min
Stop @ 30 min
Stop @ 10 min
Stop @ 0 min
0 nM
Fluorescence intensity
Time (s)
D
hit
sample
inhibitor control
negative control
% PLpro inhibition
plate #
Repeat 1
Repeat 2
Repeat 3
E
Signal : background
plate #
Repeat 1
Repeat 2
Repeat 3
F
robust Z'
plate #
Repeat 1
Repeat 2
Repeat 3

Figure EV4.

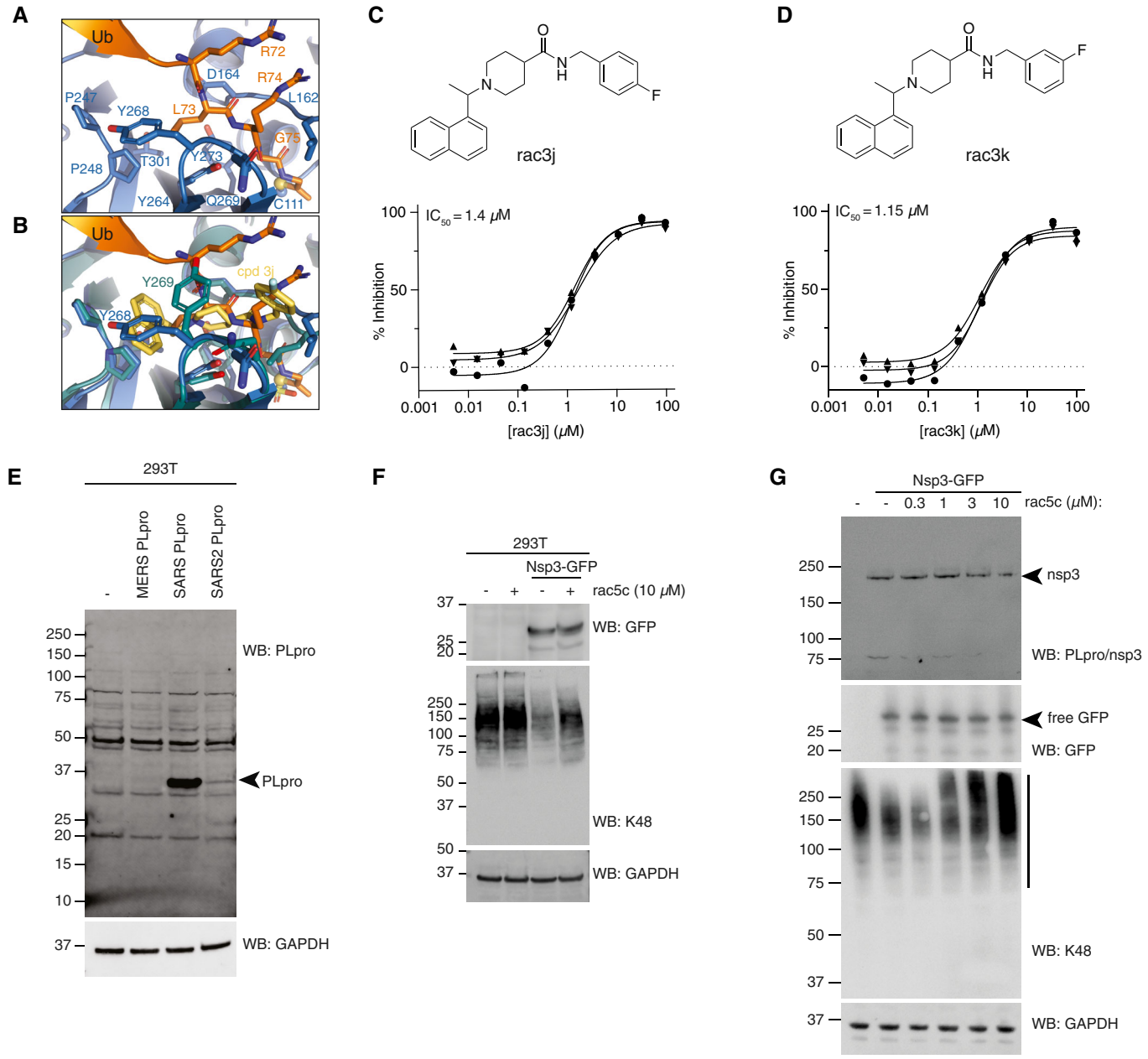

Figure EV5. SARS PLpro compounds inhibit SARS2 PLpro.

A Structure of SARS2 PLpro bound to the ubiquitin C-terminal tail in the active site, compare with Fig 5A.

B Superposition of ubiquitin tail in SARS2 PLpro, and compound 3j in SARS PLpro (pdb 4ovz (Baez-Santos *et al*, 2014)) shows an identical binding for compounds in SARS2 PLpro and highlights the change in Tyr268/269 in SARS2 PLpro and SARS PLpro, respectively.

C, D Compounds rac3j and rac3k, racemic versions of 3j and 3k from (Baez-Santos *et al*, 2014), and their *in vitro* biochemical IC_{50} values determined by the HTS assay technical triplicate and in three independent experiments (as for rac5c in Fig 5C).

E Immunoblot characterisation of the PLpro antibody on HEK 293T cells overexpressing PLpro from MERS, SARS or SARS2. Cell lysates were immunoblotted 48 h post-transfection. PLpro antibody is cross-reactive with SARS and SARS2, but not MERS PLpro.

F Immunoblot analysis showing the effect of rac5c (10 μM for 24 h) on Lys48-polyubiquitin chain disassembly by nsp3, 48 h post-transfection in HEK 293T cells. In this experiment, nsp3 expression was inferred by release of free GFP. Importantly, rac5c has no effect on global Lys48 chains in untransfected HEK293T cells.

G Experiment as in Fig 5D, with a clearer effect of nsp3 on K48-linked polyubiquitin.

Source data are available online for this figure.

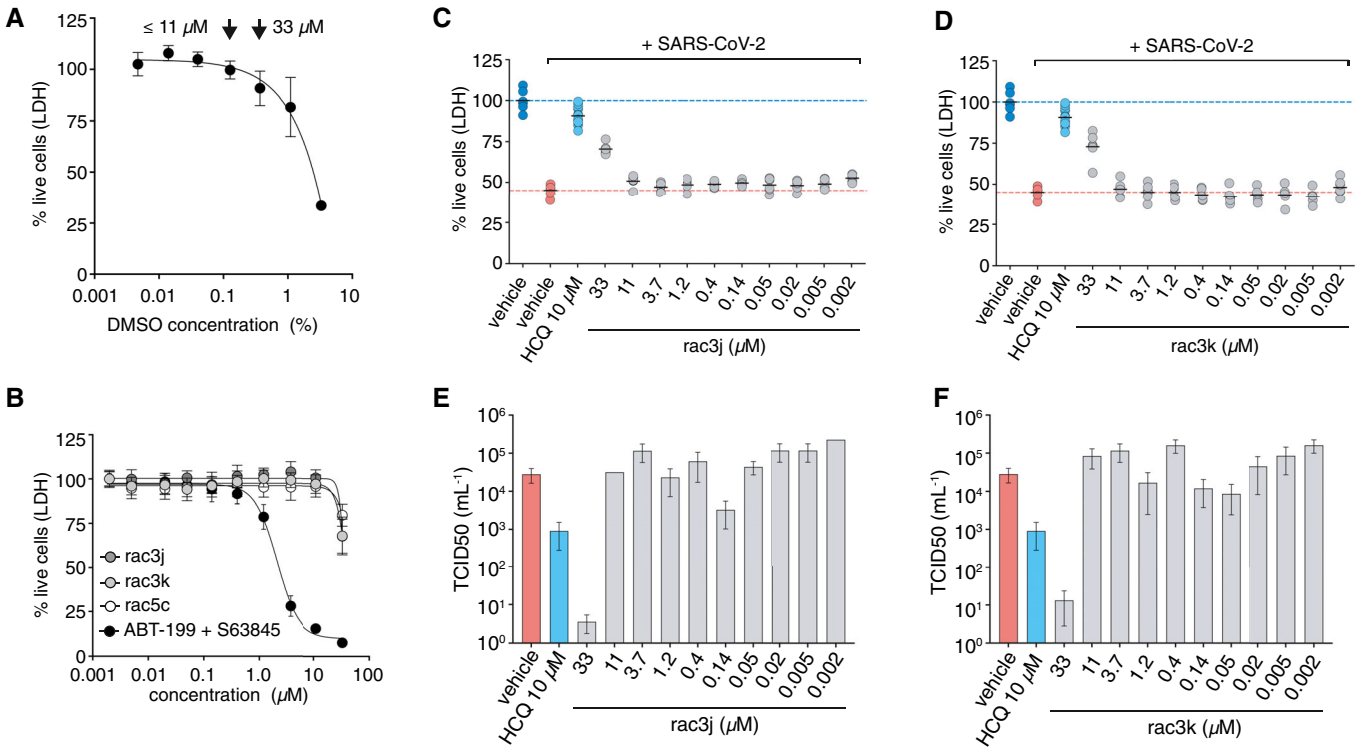

Figure EV6. Antiviral activity of compounds in cells.

A Vero cells were tested for compatibility with DMSO concentrations, revealing low toxicity at concentrations < 0.1% (*v*/*v*) but more substantial cytotoxicity at higher concentrations (0.3% and above). This limited the range of compound concentrations useable for infection studies; at concentrations up to 11 μM, 0.1% (*v*/*v*) DMSO was used as vehicle, at 33 μM compound concentration, 0.3% (*v*/*v*) DMSO was used. Higher concentrations of compound could not be tested due to this limitation. Data represent mean values ± SD from $n = 12$ technical replicates pooled from $n = 2$ independent experiments.

B Toxicity titration of compounds rac3j, rac3k and rac5c on Vero cells. At 33 μM compound concentration, cellular toxicity is ~ 25%. ABT-199 and S63845 are death-inducing compounds (Souers *et al*, 2013; Kotschy *et al*, 2016) used as a control. Data are shown as mean ± SD with $n = 12$ technical replicates pooled from $n = 2$ independent experiments for rac3j, rac3k and the controls (ABT-199 and S63845) and $n = 18$ technical replicates pooled from $n = 3$ independent experiments for rac5c.

C, D CPE assays to assess cell killing activity of SARS-CoV-2 in Vero cells left untreated (DMSO control) or treated with compounds rac3j (C) and rac3k (D). One experiment with 6 biological replicates is shown (black line, mean), and compared to HCQ-treated cells (10 μM) with pooled data from 2 experiments with $n = 6$, as in Fig 6B. The 33 μM compound concentration was performed at 0.3% (*v*/*v*) DMSO and significantly rescued infected cells despite underlying cytotoxicity in Vero cells (see A, B).

E, F TCID50 analysis of infectious virus for rac3j, rac3k, from the experiments performed in (C) and (D), respectively. Data are representative of 1 experiment out of 2, with $n = 6$ per experiment, bars represent the mean TCID50 value with error bars showing SD. HCQ control was performed within the same experiment.